THE JOURNAL OF PHYSICAL CHEMISTRY B

pubs.acs.org/JPCB Article

Twisting of Charged Nanoribbons to Helicoids Driven by Electrostatics

Gervasio Zaldivar, Martin Conda-Sheridan, and Mario Tagliazucchi*

Cite This: https://dx.doi.org/10.1021/acs.jpcb.0c01301 Read Online

ACCESS | Metrics & More | Article Recommendations | Supporting Information

ABSTRACT: Charged amphiphiles in solution usually self-assemble into flat nanoribbons that spontaneously twist into different shapes. The role of electrostatics in this process is still under strong debate. This work studies the electrostatic free energy of twisting a nanoribbon at the level of the nonlinear Poisson−Boltzmann approximation. It is shown that helicoid-shaped ribbons are more stable than flat ribbons, while other shapes under consideration (cylindrical helixes and bent ribbons) are always less stable than the flat ribbon. The unexpected electrostatics-driven twisting of the ribbon into a helicoid is ascribed to the increase in its perimeter with increasing degree of twisting, as charges near the edge of the ribbon are electrostatically more stable than those near its center. This argument successfully explains the effects of salt concentration and the width of the ribbon on the optimal twisting period and allows us to approximately describe the problem of ribbon twisting in terms of two dimensionless variables that combine the helicoid twisting period, the Debye length of the solution, and the width of the ribbon. The magnitude of the electrostatic twisting energy predicted by our calculations is comparable to that of restoring elastic forces for typical ribbons of self-assembled amphiphiles, which indicates that electrostatics plays an important role in determining the equilibrium shape of charged nanoribbons.

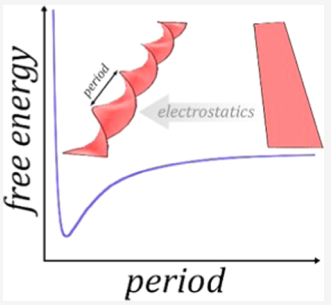

INTRODUCTION

Thin nanoribbons are a typical outcome of the self-assembly of amphiphilic molecules in solution,[1−5] such as amyloid peptides and synthetic peptide amphiphiles. Nanoribbons could further twist forming a variety of supramolecular morphologies, including helicoids (twisted ribbons)[3,6−9] or helixes (helical ribbons),[7,9,10] among other possibilities. There is reasonable consensus in the literature that chiral interactions between the molecules forming the supramolecular assembly promote twisting.[2,3,9,11,12] In this description, the intrinsic chirality of the molecules allegedly generates chiral twisted nanostructures. For example, it was proposed that ribbons formed by amphiphilic peptides twist because of the misalignment of hydrogen-bond acceptors and donors due to the chirality of the molecule.[13] The emergence of nanoscale chirality from molecular-scale chirality was profusely studied by different theoretical approaches that consider the chiral elastic properties of the ribbons.[14−18] Recently, Zhang *et al.*[19] developed a remarkably predictive model of the twisting of self-assembled ribbons based on continuum mechanics. They showed that the torsion of ribbons arises from the competition between hydrogen-bond interactions that present a preferable torsion angle and hydrophobic attractive interactions that minimize their energy in the absence of torsion.

The role of electrostatic interactions in nanoribbon twisting is much more controversial than that of molecular chirality. Electrostatic interactions, which are intrinsically nonchiral, have been shown to play a relevant role in nanoscale twisting: it has been reported that the state of charge of the molecules[7,20] and the ionic strength of the solution[4,21,22] affect the morphology of twisted ribbons. Furthermore, Hu *et al.* have shown that pure negatively or positively charged amphiphilic peptides aggregate into twisted ribbons; however, a 1:1 mixture of both amphiphiles forms flat nanobelts.[5] These experiments renew the interest in understanding how electrostatic interactions affect the morphology of ribbon-like nanoassemblies, a fundamental question that remains largely unanswered.

In the past, the role of electrostatic interactions in the twisting of nanoribbons was theoretically studied using chiral polarization effects,[23] scaling arguments,[24] approximate analytical solutions of the Poisson−Boltzmann (PB) equation,[4] and simulations using pairwise-additive screened coulombic interactions (Yukawa potential) between point charges.[25] In this report, we present the first study to decipher the role of electrostatics in twisting based on solving the fully nonlinear Poisson−Boltzmann (PB) equation.[26,27] This model predicts the electrostatic contributions to the free energy of the system for a surface immersed in an electrolyte solution. Importantly, we avoid simplifications such as the linearization of the PB equation or the assumption of pairwise additivity.

Received: February 14, 2020
Revised: March 18, 2020
Published: March 23, 2020

ACS Publications © XXXX American Chemical Society

METHODS

Theoretical Methods. The thermodynamic potential that describes the electrostatic contribution to the free energy of a charged ribbon in a salt solution is the grand-canonical potential $\Omega(T, V, \{\mu_i\}, N_q)$,[28] which considers a system at constant temperature (T), volume (V), chemical potential of the free ions (μ_i), and number of fixed charges ($N_q = A\cdot\sigma$, where A is the surface area). This potential is

$$\beta\Omega = \sum_{i=a,c}\int \rho_i(\mathbf{r})[\ln(\rho_i(\mathbf{r})/\rho^0) - 1]d\mathbf{r} + \beta\sum_{i=a,c}\int \rho_i(\mathbf{r})(\mu_i^0 - \mu_i)d\mathbf{r} + \beta\int\left[\left(\sum_i \rho_i(\mathbf{r})q_i\right)\varphi(\mathbf{r}) - \frac{\varepsilon_r\varepsilon_0}{2}(\nabla\varphi(\mathbf{r}))^2\right] d\mathbf{r} + \beta\int_S \varphi(\mathbf{r})\sigma\, d\mathbf{S} \quad (1)$$

where $\rho_i(\mathbf{r})$ is the number density of the ions at position $\mathbf{r}$ (i = a, c for anions and cations, respectively), ρ^0 is a reference density (whose choice does not have thermodynamic consequences), $\varphi(\mathbf{r})$ is the electrostatic potential at position $\mathbf{r}$, $\beta = 1/k_BT$ (k_B is Boltzmann's constant), $q_i = |e|$ and $-|e|$ for i = c and a, respectively ($|e|$ is the elemental charge), ε_0 is the vacuum's dielectric permittivity, and ε_r is the relative dielectric permittivity (we use water's value at 25 °C, ε_r = 78.5). Each term in eq 1 represents a contribution to the grand free energy. The first term is the free energy associated with the mixing entropy of the anions and cations. The second term is the energy associated with the chemical potential of the ions. The third and fourth terms are the electrostatic contributions to the free energy associated with the volume charge density of the solution and the surface charge density of the ribbon, respectively.

The equilibrium properties of the system are determined by finding the functional extremum of Ω with respect to $\rho_i(\mathbf{r})$ and $\varphi(\mathbf{r})$. This procedure results in the well-known PB equation[26,27]

$$\nabla^2\varphi(\mathbf{r}) = -\frac{\sum_i \rho_i(\mathbf{r})q_i}{\varepsilon_0\varepsilon_r} \quad (2)$$

with

$$\rho_i(\mathbf{r}) = \rho_i^{bulk}\exp(-\beta q_i(\mathbf{r})) \quad (3)$$

The boundary conditions of eq 2 are

$$\varphi^{bulk} = 0 \quad (4)$$

and on the ribbon surface

$$\nabla_n\varphi(S) = -\frac{\sigma}{\varepsilon_r\varepsilon_0} \quad (5)$$

We solved eqs 2−5 using the finite-element method (FEM) implemented in COMSOL Multiphysics 5.2 (the Supporting Information (SI) describes details of the implementation, control calculations, and convergence tests). The calculation was performed by enforcing periodic boundary conditions in the long axis of the ribbon; therefore, we are effectively modeling infinite ribbons. The value of $\Omega(T, V, \{\mu_i\}, N_q)$ at its extreme, which results from inserting the values of $\rho_i(\mathbf{r})$ and $\varphi(\mathbf{r})$ that satisfy eqs 2−5 into eq 1, is a criterion of thermodynamic stability,[28] *i.e.*, for fixed T, V, μ_i, and N_q; smaller values of Ω indicate a more stable structure. To assess the relative stability of systems within calculation boxes having different V and N_q, we compared the excess value of Ω per unit area of the surface, Ω^*, which, as explained in the Supporting Information of ref 29, is the proper thermodynamic potential to compare the thermodynamic stability of infinitely long ribbons.

RESULTS AND DISCUSSION

We calculate the free energy of thin, long nanoribbons of different shapes (helicoids, helixes, longitudinally and transversally bent ribbons, and flat ribbons; see Figure 1) immersed in a 1:1 electrolyte aqueous solution. The parameters characterizing these shapes are the salt concentration of the solution, the width of the ribbon (w), its surface charge density (σ), and its state of deformation. The latter is defined by the period of twisting (P) for helicoid-shaped ribbons, the period of twisting (P) and radius (r) for helical ribbons, the angle of bending (α) for longitudinally bent ribbons, and the amplitude of bending (a) for transversally bent ribbons. Figure 1 shows representations of the considered shapes, where the parameters that define the state of deformation are marked with blue double arrows.

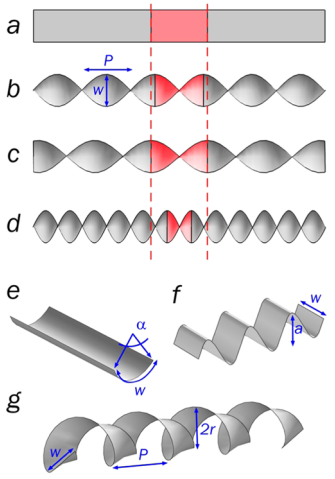

Figure 1. Representation of a flat ribbon (a), helicoid-shaped ribbons (b−d), a longitudinally bent ribbon (e), a transversally bent ribbon (f), and a helical ribbon (g). The red shaded region in (a)−(d) defines ribbon-to-helicoid transformations that conserve the area of this region (b), its length (c), or its contour length, *i.e.*, perimeter not including the lines normal to the edge of the ribbon (d). The width is constant in the three transformations. Blue arrows indicate the relevant geometric parameters for each morphology.

The twisting of a flat nanoribbon to a helicoid can be performed under different conditions. The most reasonable assumption for nanoribbons self-assembled from amphiphilic molecules is to fix the width of the ribbon and its area, *i.e.*, a transformation that keeps the area of the red region in the flat ribbon shown in Figure 1a fixed when twisting it into the helicoid in Figure 1b. The constant-width assumption is reasonable for self-assembled ribbons because the width is fixed by the number of molecules along the short axis of the ribbon. The constant-area transformation is also reasonable as it is equivalent to fixing the intermolecular distances within the ribbon, which are mainly determined by interactions at the

https://dx.doi.org/10.1021/acs.jpcb.0c01301
J. Phys. Chem. B XXXX, XXX, XXX−XXX

molecular scale. As a corollary, a constant-area transformation will keep the surface charge density of the ribbon fixed. Besides constant-area twisting, one can also envisage constant-perimeter and constant-length twisting (helicoids in Figure 1c,d), but these transformations are unphysical for self-assembled nanoribbons. Therefore, in the discussion below, we will focus on the constant-area transformation and report the results for the constant-perimeter and constant-length twisting in the Supporting Information (SI).

In our model, we approximated very thin and long nanoribbons as infinitely long charged surfaces with no thickness. The surface is immersed in a solution of mobile ions with a constant chemical potential fixed by the salt concentration of the bulk solution (*i.e.*, very far from the surface). We considered only the electrostatic contributions to the free energy (see Methods) because we are interested in understanding how purely electrostatic effects affect twisting. Therefore, the results discussed below do not include contributions from elastic deformations and they describe a physically meaningful system only in the limit where electrostatic interactions dominate over elastic effects. At the end of this work, we compare the electrostatic and the elastic contributions and show that their order of magnitude is comparable; therefore, in the most likely scenario, none of these contributions are negligible.

Figure 2a shows the change of Ω^* for the constant-area transformation of a charged flat ribbon into a helicoid ($\Delta\Omega^* = \Omega^*_{\text{helicoid}} - \Omega^*_{\text{flat ribbon}}$) as a function of the period of twisting (P) for different salt concentrations. Note that, in this plot, a helicoid with $P \to \infty$ is equivalent to the flat ribbon; therefore, $\Delta\Omega^* \to 0$ as $P \to \infty$. Figure 2a shows that, for all values of salt concentration, $\Delta\Omega^*$ has a minimum as a function of P. Therefore, at the equilibrium twisting period, P_{eq}, the helicoid is more stable than the flat ribbon. This observation is the most important result of this work, as it shows that electrostatics spontaneously promotes the twisting of a charged ribbon in solution.

It is important to stress that the shape of the ribbon is fixed during the calculations, and, therefore, our theory does not include the effects of thermal fluctuations on the shape. In the absence of chiral interactions, thermal fluctuations may affect long-range order in the system because electrostatically induced twisting can produce left-handed and right-handed helicoids with equal probability. On the other hand, if the chirality of the ribbon is fixed by molecular chirality, thermal effects produce a distribution of twisting periods around the optimal value observed in Figure 2a.[18,19] In the SI, we include a more detailed analysis of how the thermal fluctuations affect the twisting period of ribbons in the latter case.

It is important to mention that, of all of the different shapes considered in Figure 1, the helicoid-shaped ribbon is the only structure that is more stable than the flat ribbon (see the SI). For example, for helical ribbons, $\Delta\Omega^*$ monotonically decreases with the helix period for a fixed radius. This result is in agreement with experimental observations that show that charge screening[30] and pH-driven neutralization[7] disfavor the formation of helical ribbons. We believe that the special stability of the helicoid may be originated in the fact that the helicoid and the flat ribbon are minimal surfaces (they have zero mean curvature), while the other structures in Figure 1 are not.[31]

We hypothesize that the stability of the helicoid with respect to the nontwisted ribbon arises from the competition between

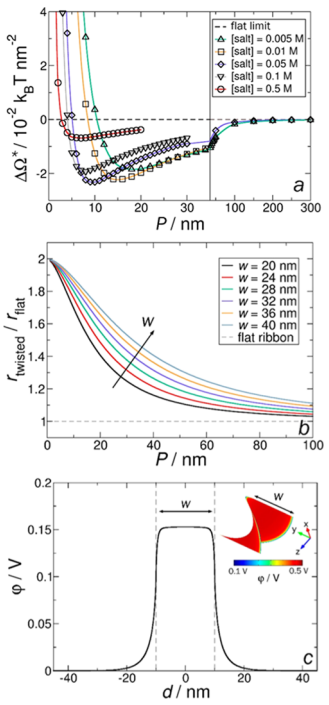

Figure 2. (a) Excess free energy per unit area for the transition of a charged flat ribbon into a helicoid ($\Delta\Omega^*$) as a function of the period of twisting (P), for different salt concentrations. Calculations were performed at a constant ribbon area. Note that the vertical solid line separates two different scales of P. (b) Perimeter-to-area ratio of a twisted ribbon (r_{twisted}) relative to that of a flat ribbon (r_{flat}) as a function of the period of twisting, for different values of ribbon or in a highly saline condition width. (c) Electrostatic potential (φ) as a function of the distance to the center of the ribbon (d) along a line normal to the edge of the ribbon (line with arrows in the inset). Gray dashed lines show the lateral boundaries of the ribbon. The inset shows a color map of φ at the surface of the ribbon. Calculation parameters: w = 20 nm, σ = 1 |e|·nm^{-2}, salt concentration = 0.005 M (panel c).

two opposite electrostatic effects. On the one hand, increasing the degree of twisting (*i.e.*, decreasing period) decreases the average distance between charges, which increases the electrostatic repulsions. This effect clearly destabilizes twisted structures. On the other hand, the perimeter-to-area ratio of the helicoid increases with decreasing P; see Figure 2b. In particular, a helicoid has a larger perimeter-to-area ratio than a flat ribbon of the same width and area. Charges at the edge of the ribbon experience less electrostatic repulsions than those located at its center because a charge at the ribbon edge can accommodate a double layer of oppositely charged ions more effectively than a central charge. This mechanism is supported by Figure 2c, which shows that the electrostatic potential, φ, in the edge of the structure is smaller than near its center because edge charges are more screened by the electrolyte than center charges. As a conclusion, the increase of the perimeter-to-area ratio with decreasing P stabilizes the twisted structure. The two opposing effects discussed above give rise to the minimum in the $\Delta\Omega^*(P)$ plot.

Figure 2a shows that the equilibrium period, P_{eq}, monotonically decreases as the salt concentration increases. The absolute value of $\Delta\Omega^*(P_{eq})$, on the other hand, experiences a maximum for a salt concentration of around 0.05 M. For salt concentrations much larger than 0.05 M, electrostatic interactions become negligible due to screening by the salt

https://dx.doi.org/10.1021/acs.jpcb.0c01301
J. Phys. Chem. B XXXX, XXX, XXX−XXX

ions, which decreases $\Delta\Omega^*$. For salt concentrations much lesser than 0.05 M, the equilibrium shape tends to the flat ribbon because $P_{eq} \rightarrow \infty$; therefore, $\Delta\Omega^*(P_{eq})$ should also vanish. Interestingly, twisting is not predicted to occur both in the absence of electrolyte ($P_{eq} \rightarrow \infty$ for [salt] $\rightarrow$ 0) or in highly saline conditions ($\Delta\Omega^*(P_{eq}) \rightarrow 0$ for [salt] $\rightarrow \infty$).

We next analyzed how the equilibrium period, P_{eq}, is affected by the width of the ribbon, w, at different salt concentrations (Figure 3a). For all salt concentrations, the equilibrium period

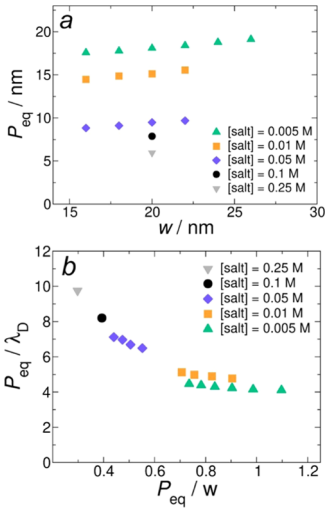

Figure 3. (a) Equilibrium period, P_{eq}, as a function of the width of the ribbon, w, for different salt concentrations. (b) Equilibrium period divided by the Debye length, P_{eq}/λ_D, as a function of the equilibrium period divided by the width of the ribbon, P_{eq}/w. Both plots use the same color code.

increases approximately linearly with the width. This result qualitatively agrees with the experimental observation of an increase in the twisting period with ribbon width in self-assembled peptide amphiphiles.[8,32] The effect of w on P_{eq} can be rationalized in terms of our hypothesis of two competing electrostatic effects that dictate the value of P_{eq}. A decrease in w results in a decrease of the perimeter-to-area ratio (compared to that of a flat ribbon of the same width; see Figure 2b). Therefore, the system responds, increasing its perimeter-to-area ratio by decreasing P_{eq}. This mechanism explains the increase of P_{eq} with increasing w.

The characteristic length scales involved in the twisting of infinitely long and thin nanoribbons into helicoids are the width (w), the equilibrium period (P_{eq}), and the Debye length of the solution (λ_D, the Debye length is a characteristic length scale for electrostatic interactions in an electrolyte solution and scales as $\lambda_D \sim [\text{salt}]^{-1/2}$). The nonlinearity of the problem and the complexity of the geometry preclude an exact analytical solution of the PB equation, so it is not possible to exactly cast the problem in terms of dimensionless variables involving these length scales. However, approximately universal behaviors may exist and can be explored numerically. We propose above that the perimeter-to-area ratio is one of the two effects controlling the degree of twisting. In the SI, we show that this parameter depends only on the ratio between the equilibrium period and width of the helicoid, P_{eq}/w.

The second proposed effect that determines the degree of twisting is the decrease of the average distance between charges with decreasing equilibrium period. This effect is difficult to analyze, but it is reasonable to assume that it will depend on the balance between the equilibrium period (smaller P_{eq}, stronger repulsions) and the Debye length, λ_D (smaller λ_D implies stronger salt screening and weaker electrostatic repulsions). Based on these considerations, we propose that this effect is controlled by the dimensionless variable P_{eq}/λ_D. In Figure 3b, we show plots of P_{eq}/w *vs* P_{eq}/λ_D for the same calculations shown in Figure 3a. All data sets approximately collapse to a single universal curve, which supports the idea that the dimensionless parameters controlling the behavior of the system are P_{eq}/w and P_{eq}/λ_D.

Heretofore, we have shown that electrostatic repulsions spontaneously twist a charged flexible ribbon into a helicoid. To understand how relevant this result is in experimental systems, we consider next the elastic resistance of the ribbons and compare it with the electrostatic contribution. To estimate the elastic contribution, we compute the mechanical energy per unit area of a ribbon that is twisted at an angle ϕ through a length L, given by[33]

$$U_{elastic} = \frac{GI_p\phi^2}{2A_{helicoid}L} \quad (6)$$

where $G = 0.5E/(1 + \nu)$ is the shear modulus (E is Young's modulus and ν is Poisson's ratio), I_P is the torsion constant of the cross section of the ribbon that depends on its width and thickness,[34] and $A_{helicoid}$ is the area of the helicoid. Since we are considering an infinite-length ribbon, we calculated $U_{elastic}$ for a section defined by one period P; we set $L = P$, $\phi = \pi$, and $A_{helicoid}$ to be equal to the area of that section (see the SI). Note that for a given ribbon, defined by its width, thickness, and shear modulus, $U_{elastic}$ increases with increasing degree of twisting, *i.e.*, when the period decreases. For a helicoid-shaped ribbon with a period equal to 15 nm and a width equal to 20 nm, $U_{elastic}$ is 0.09 k_BT/nm^2. In this calculation, we set the thickness to 3.41 nm, Young's modulus to 9.5 MPa, and Poisson's ratio to 0.5, which correspond to the values obtained by Zhang *et al.*[19] for the elastic energy of twisted ribbons formed by a lysine-based peptide amphiphile. Figure 2a shows that the electrostatic contribution to the free energy for ribbons with a width equal to 20 nm and a salt concentration of 0.005 M is −0.02 k_BT/nm^2 (see Figure 2a). This value is less than an order of magnitude smaller than $U_{elastic}$, which implies that electrostatic effects on ribbon twisting are expected to be relevant compared to the elastic contribution. It is important to mention that $U_{elastic}$ strongly depends on the elastic and geometric properties of the ribbon. The elastic energy will be small for thin ribbons (which are more flexible than thick ones), small shear modulus, and large twisting periods (which occur at small salt concentrations; see Figure 2a). In such cases, electrostatics should be taken explicitly into account to understand how the shape of self-assembled ribbons arises.

Ribbons often present a preferred angle of torsion ϕ_0 due to chiral interactions at the molecular level[2,19] (note that in eq 6, $\phi_0 = 0$). In these cases, $U_{elastic}$ increases when the angle of torsion shifts away from ϕ_0, and ϕ_0 hence defines an elastic equilibrium period. Since the order of magnitude of the elastic energy is similar to that of the electrostatic energy near the electrostatic equilibrium period, electrostatics should be taken into account if the period given by ϕ_0 is close to the period given by electrostatics, which, for the systems analyzed in this work, is ∼10−20 nm. This conclusion is supported by

https://dx.doi.org/10.1021/acs.jpcb.0c01301
J. Phys. Chem. B XXXX, XXX, XXX−XXX

experimental data. For example, Adamcik and Mezzenga[4] showed that the salt concentration tunes the period of twisted amyloid fibrils in the range of 25−200 nm. Furthermore, Uesaka *et al.*[7] prepared twisted and helical ribbons of different twisting periods (∼50−100 nm) by pH-driven charge regulation. On the contrary, when the twisting period is much larger than the optimum period dictated by electrostatics, charge regulation is expected to play a minor role or not to play a role at all. In sum, we conclude that the shape of flexible ribbons that present a periodic torsion with relatively small pitch will be significantly affected by electrostatic interactions.

Finally, we investigated if an approximated description of the electrostatic interactions using a pairwise-additive potential can capture the fact that helicoids are minimum free-energy surfaces in electrolyte solutions. More specifically, we consider the Yukawa potential, which models the electrostatic potential generated by a point charge in an electrolyte solution at the level of the linearized PB equation.[26,35] Under the assumption of pairwise additivity, this potential is usually used to model systems with more than a single charge. To compute the pairwise Yukawa energy of a charged ribbon, we defined point charges homogeneously distributed on the ribbon surface and computed the total Yukawa free energy, given by

$$\Omega_{\text{Yukawa}} = \frac{|e|^2}{4\pi\varepsilon_0\varepsilon_r}\sum_j \sum_{i>j, r_{ij}>r_0} \frac{\exp(-(r_{ij}-r_0)/\lambda_D}{r_{ij}(1+r_0/\lambda_D)} \quad (7)$$

where r_{ij} is the distance between charges i and j, r_0 is the minimum allowed distance between two charges, and λ_D is the Debye length. For the calculations shown below, we set r_0 to 1 nm, but our qualitative conclusions are independent of the value of this parameter.

Figure 4 shows the Yukawa free-energy difference per unit area between a helicoid and a flat ribbon, $\Delta\Omega_{\text{Yukawa}}$, as a function of the period of twisting of the helicoid (P), for different salt concentrations. As expected, $\Delta\Omega_{\text{Yukawa}}$ tends to zero for $P \to \infty$. For all P, $\Delta\Omega_{\text{Yukawa}}$ is positive; therefore, the Yukawa model predicts that the twisted ribbon is always less stable than the flat ribbon. Note that, in a previous model from de la Cruz's group that used Yukawa interactions,[25] helicoids were more stable than flat ribbons in some conditions; however, that model considered harmonic forces between charges in addition to electrostatics. We also note that the order of magnitude of $\Delta\Omega_{\text{Yukawa}}$ (Figure 4) is significantly larger than that predicted by the PB calculation (Figure 1a). This difference between the pairwise-additive Yukawa model and the PB calculations seems to be a general characteristic, as we show in the SI by analyzing the free energy between two infinite charged planes using numerical and analytical PB calculations and the Yukawa model. We ascribe the qualitative and quantitative differences between the predictions of the full PB approach and the pairwise-additive approximation to the fact that the latter does not take into account the nonadditivity of the ionic double layers surrounding the fixed charges of the helicoid.

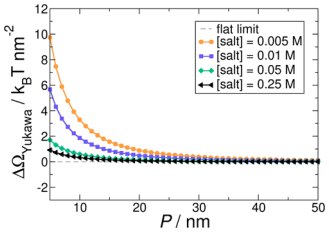

Figure 4. Difference between the Yukawa free energies of a twisted ribbon and a flat ribbon ($\Delta\Omega_{\text{Yukawa}}$) as a function of the period of twisting (P). Calculation parameters: w = 20 nm, σ = 1 $|e|\cdot nm^{-2}$.

CONCLUSIONS

In summary, we have shown that charged helicoids are more stable than flat ribbons in electrolyte solutions under the assumption of a constant-area transformation. This transformation is the most reasonable one as it keeps a constant charge density, σ. The stabilizing electrostatic free energy for twisting the ribbon and the elastic energetic penalty have similar orders of magnitude. In the case of nanoribbons formed by amphiphile self-assembly, the electrostatic contributions will be relevant for flexible ribbons (thin ribbons with low Young's modulus), large surface charge densities (highly charged amphiphiles), and low ionic strengths (which promote large twisting periods that involve low elastic penalties). Even in the case where the spontaneous twisting of the ribbon results from molecular chirality, electrostatic interactions may be relevant and shift the optimal twisting period. This situation can be recognized in experiments as a dependence of the twisting period on the ionic strength of the solution.

The fact that the helicoid is a minimum free-energy surface in aqueous solution is unexpected if we consider that a one-dimensional string of charges minimizes its energy in the fully stretched conformation. However, twisting the nanoribbon into a helicoid (keeping a constant and homogeneous charge density) results in an increase in its perimeter. We, therefore, ascribe the stability of the helicoid to an increase in the number of charges near the edge, which are more stable than those near the axis. This simple argument successfully explains many of our numerical results, but one should note that there still remain open questions, for example, why the helicoid is the only twisted shape that can be more stable than the flat ribbon and why pairwise-additive electrostatic models fail to capture the effect. In conclusion, the results of this work provide new insights into the role of electrostatics in the shape development of soft materials.

ASSOCIATED CONTENT

Supporting Information

The Supporting Information is available free of charge at https://pubs.acs.org/doi/10.1021/acs.jpcb.0c01301.

Numerical implementation, constant-perimeter and constant-length twisting results, analysis of the stability of ribbons of other shapes, the analytical expression of the perimeter-to-area ratio of a helicoid, and the comparison between numerical and analytical Poisson−Boltzmann calculations and Yukawa approximation for the free energy of opposing charged surfaces (PDF)

AUTHOR INFORMATION

Corresponding Author

Mario Tagliazucchi − *Instituto de Química Física de los Materiales, Medio Ambiente y Energía and Departamento de Química Inorgánica Analítica y Química Física, University of Buenos Aires, School of Sciences, Ciudad Universitaria, Ciudad Autónoma de Buenos Aires C1428EHA, Argentina;*

https://dx.doi.org/10.1021/acs.jpcb.0c01301
J. Phys. Chem. B XXXX, XXX, XXX−XXX

orcid.org/0000-0003-4755-955X; Email: mario@qi.fcen.uba.ar

Authors

Gervasio Zaldivar − *Instituto de Química Física de los Materiales, Medio Ambiente y Energía and Departamento de Química Inorgánica Analítica y Química Física, University of Buenos Aires, School of Sciences, Ciudad Universitaria, Ciudad Autónoma de Buenos Aires C1428EHA, Argentina*

Martin Conda-Sheridan − *Department of Pharmaceutical Sciences, College of Pharmacy, University of Nebraska Medical Center, Omaha, Nebraska 68198-6125, United States;* orcid.org/0000-0002-3568-2545

Complete contact information is available at: https://pubs.acs.org/10.1021/acs.jpcb.0c01301

Notes

The authors declare no competing financial interest.

■ ACKNOWLEDGMENTS

M.T. is a fellow of CONICET. M.T. acknowledges financial support from Agencia Nacional de Promoción Científica y Tecnológica (ANPCyT) PICT 0154-2016 and the University of Buenos Aires (UBACYT 20020170200215BA). The authors acknowledge a CONICET-NIH Level 1 Bilateral Cooperation Grant. M.C.-S. acknowledges support from the American Chemical Society-Petroleum Research Fund (ACS-PRF# 57434-DNI7, M.C.-S.). This work was completed with the help of the Holland Computing Center of the University of Nebraska, which receives support from the Nebraska Research Initiative.

■ REFERENCES

(1) Cui, H.; Muraoka, T.; Cheetham, A. G.; Stupp, S. I. Self-Assembly of Giant Peptide Nanobelts. *Nano Lett.* **2009**, *9*, 945−951.

(2) Oda, R.; Huc, I.; Schmutz, M.; Candau, S. J.; MacKintosh, F. C. Tuning Bilayer Twist Using Chiral Counterions. *Nature* **1999**, *399*, 566.

(3) Douliez, J.-P.; Navailles, L.; Nallet, F.; Gaillard, C. Self-Assembly of Unprecedented Swollen Multilamellar Twisted Ribbons from a Racemic Hydroxy Fatty Acid. *ChemPhysChem* **2008**, *9*, 74−77.

(4) Adamcik, J.; Mezzenga, R. Adjustable Twisting Periodic Pitch of Amyloid Fibrils. *Soft Matter* **2011**, *7*, 5437−5443.

(5) Hu, Y.; Lin, R.; Zhang, P.; Fern, J.; Cheetham, A. G.; Patel, K.; Schulman, R.; Kan, C.; Cui, H. Electrostatic-Driven Lamination and Untwisting of β-Sheet Assemblies. *ACS Nano* **2016**, *10*, 880−888.

(6) Mason, M. L.; Lalisse, R. F.; Finnegan, T. J.; Hadad, C. M.; Modarelli, D. A.; Parquette, J. R. PH-Controlled Chiral Packing and Self-Assembly of a Coumarin Tetrapeptide. *Langmuir* **2019**, *35*, 12460−12468.

(7) Uesaka, A.; Ueda, M.; Makino, A.; Imai, T.; Sugiyama, J.; Kimura, S. Morphology Control between Twisted Ribbon, Helical Ribbon, and Nanotube Self-Assemblies with His-Containing Helical Peptides in Response to PH Change. *Langmuir* **2014**, *30*, 1022−1028.

(8) Ziserman, L.; Mor, A.; Harries, D.; Danino, D. Curvature Instability in a Chiral Amphiphile Self-Assembly. *Phys. Rev. Lett.* **2011**, *106*, No. 238105.

(9) Zhang, L.; Wang, T.; Shen, Z.; Liu, M. Chiral Nanoarchitectonics: Towards the Design, Self-Assembly, and Function of Nanoscale Chiral Twists and Helices. *Adv. Mater.* **2016**, *28*, 1044−1059.

(10) Pashuck, E. T.; Stupp, S. I. Direct Observation of Morphological Tranformation from Twisted Ribbons into Helical Ribbons. *J. Am. Chem. Soc.* **2010**, *132*, 8819−8821.

(11) Wang, X.; Hao, J. Ionogels of Sugar Surfactant in Ethylammonium Nitrate: Phase Transition from Closely Packed Bilayers to Right-Handed Twisted Ribbons. *J. Phys. Chem. B* **2015**, *119*, 13321−13329.

(12) Shimizu, T.; Masuda, M.; Minamikawa, H. Supramolecular Nanotube Architectures Based on Amphiphilic Molecules. *Chem. Rev.* **2005**, *105*, 1401−1444.

(13) Aggeli, A.; Nyrkova, I. A.; Bell, M.; Harding, R.; Carrick, L.; McLeish, T. C. B.; Semenov, A. N.; Boden, N. Hierarchical Self-Assembly of Chiral Rod-like Molecules as a Model for Peptide β-Sheet Tapes, Ribbons, Fibrils, and Fibers. *Proc. Natl. Acad. Sci. U.S.A.* **2001**, *98*, 11857−11862.

(14) Nandi, N.; Bagchi, B. Molecular Origin of the Intrinsic Bending Force for Helical Morphology Observed in Chiral Amphiphilic Assemblies: Concentration and Size Dependence. *J. Am. Chem. Soc.* **1996**, *118*, 11208−11216.

(15) Selinger, J. V.; Spector, M. S.; Schnur, J. M. Theory of Self-Assembled Tubules and Helical Ribbons. *J. Phys. Chem. B* **2001**, *105*, 7157−7169.

(16) Ghafouri, R.; Bruinsma, R. Helicoid to Spiral Ribbon Transition. *Phys. Rev. Lett.* **2005**, *94*, No. 138101.

(17) Selinger, R. L. B.; Selinger, J. V.; Malanoski, A. P.; Schnur, J. M. Shape Selection in Chiral Self-Assembly. *Phys. Rev. Lett.* **2004**, *93*, No. 158103.

(18) Grossman, D.; Sharon, E.; Diamant, H. Elasticity and Fluctuations of Frustrated Nanoribbons. *Phys. Rev. Lett.* **2016**, *116*, No. 258105.

(19) Zhang, M.; Grossman, D.; Danino, D.; Sharon, E. Shape and Fluctuations of Frustrated Self-Assembled Nano Ribbons. *Nat. Commun.* **2019**, *10*, No. 3565.

(20) Shao, H.; Parquette, J. R. Controllable Peptide−Dendron Self-Assembly: Interconversion of Nanotubes and Fibrillar Nanostructures. *Angew. Chem., Int. Ed.* **2009**, *48*, 2525−2528.

(21) Cuvier, A.-S.; Babonneau, F.; Berton, J.; Stevens, C. V.; Fadda, G. C.; Genois, I.; Griel, P. L.; Péhau-Arnaudet, G.; Baccile, N. Synthesis of Uniform, Monodisperse, Sophorolipid Twisted Ribbons. *Chem. - Asian J.* **2015**, *10*, 2419−2426.

(22) Castelletto, V.; Hamley, I. W.; Cenker, C.; Olsson, U. Influence of Salt on the Self-Assembly of Two Model Amyloid Heptapeptides. *J. Phys. Chem. B* **2010**, *114*, 8002−8008.

(23) Chappell, J. S.; Yager, P. Electrostatic Interactions within Helical Structures of Chiral Lipid Bilayers. *Chem. Phys.* **1991**, *150*, 73−79.

(24) Adamcik, J.; Jung, J.-M.; Flakowski, J.; Rios, P. D. L.; Dietler, G.; Mezzenga, R. Understanding Amyloid Aggregation by Statistical Analysis of Atomic Force Microscopy Images. *Nat. Nanotechnol.* **2010**, *5*, 423−428.

(25) Yao, Z.; de la Cruz, M. O. Electrostatics-Driven Hierarchical Buckling of Charged Flexible Ribbons. *Phys. Rev. Lett.* **2016**, *116*, No. 148101.

(26) Walker, D. A.; Kowalczyk, B.; de la Cruz, M. O.; Grzybowski, B. A. Electrostatics at the Nanoscale. *Nanoscale* **2011**, *3*, 1316−1344.

(27) Bard, A. J.; Faulkner, L. R. *Electrochemical Methods: Fundamentals and Applications*, 2nd ed.; Wiley: New York, 2000; pp 546−547.

(28) Che, J.; Dzubiella, J.; Li, B.; McCammon, J. A. Electrostatic Free Energy and Its Variations in Implicit Solvent Models. *J. Phys. Chem. B* **2008**, *112*, 3058−3069.

(29) Zaldivar, G.; Vemulapalli, S.; Udumula, V.; Conda-Sheridan, M.; Tagliazucchi, M. Self-Assembled Nanostructures of Peptide Amphiphiles: Charge Regulation by Size Regulation. *J. Phys. Chem. C* **2019**, *123*, 17606−17615.

(30) Terech, P.; K. P. Velu, S.; Pernot, P.; Wiegart, L. Salt Effects in the Formation of Self-Assembled Lithocholate Helical Ribbons and Tubes. *J. Phys. Chem. B* **2012**, *116*, 11344−11355.

(31) Krivoshapko, S.; Ivanov, V. N. *Encyclopedia of Analytical Surfaces*, 1st ed.; Springer International Publishing: Heidelberg, 2015; pp 1−72.

(32) Moyer, T. J.; Cui, H.; Stupp, S. I. Tuning Nanostructure Dimensions with Supramolecular Twisting. *J. Phys. Chem. B* **2013**, *117*, 4604−4610.

571 (33) Gere, J. M. *Mechanics of Materials*, 6th ed.; Brooks/Cole−
572 Thomson Learning: Beltmon, CA, 2001; pp 227−228.
573 (34) Young, W. C.; Budynas, R. G.; Sadegh, A. M. *Roark's Formulas*
574 *for Stress and Strain*, 7th ed.; McGraw-Hill: New York, 2002; pp 401−
575 426.
576 (35) Israelachvili, J. N. *Intermolecular and Surface Force*, 3rd ed.;
577 Academic Press: Burlington, MA, 2011; pp 317−318.

https://dx.doi.org/10.1021/acs.jpcb.0c01301
J. Phys. Chem. B XXXX, XXX, XXX−XXX